Optoelectronic properties of bottom gate-defined in-plane monolayer WSe_2 p–n junction*

Di Liu(刘峘)[1,2], Xiao-Zhuo Qi(祁晓卓)[1,2], Kuei-Lin Chiu(邱奎霖)[1,2], Takashi Taniguchi[3], Xi-Feng Ren(任希锋)[1,2,†], and Guo-Ping Guo(郭国平)[1,2,‡]

[1] *Key Laboratory of Quantum Information, University of Science and Technology of China, Chinese Academy of Sciences, Hefei* 230026, *China*
[2] *Synergetic Innovation Center of Quantum Information & Quantum Physics, University of Science and Technology of China, Hefei* 230026, *China*
[3] *National Institute for Materials Science, Namiki* 1-1, *Ibaraki* 305-0044, *Japan*

(Received 10 March 2018; revised manuscript received 11 May 2018; published online 10 July 2018)

Monolayer transition-metal dichalcogenides (TMDs) are considered to be fantastic building blocks for a wide variety of optical and optoelectronic devices such as sensors, photodetectors, and quantum emitters, owing to their direct band gap, transparency, and mechanical flexibility. The core element of many conventional electronic and optoelectronic devices is the p–n junction, in which the p- and n-types of the semiconductor are formed by chemical doping in different regions. Here, we report a series of optoelectronic studies on a monolayer WSe_2 in-plane p–n photodetector, demonstrating a low-power dissipation by showing an ambipolar behavior with a reduced threshold voltage by a factor of two compared with the previous results on a lateral electrostatically doped WSe_2 p–n junction. The fabrication of the device is based on a polycarbonates (PC) transfer technique and hence no electron-beam exposure induced damage to the monolayer WSe_2 is expected. Upon optical excitation, the photodetector demonstrates a photoresponsivity of 0.12 mA·W^{-1} and a maximum external quantum efficiency of 0.03%. Our study provides an alternative platform for a flexible and transparent two-dimensional photodetector, from which we expect to further promote the development of next-generation optoelectronic devices.

Keywords: WSe_2, photodetector, transfer technique, p–n junction

PACS: 73.40.Lq, 85.60.Dw **DOI:** 10.1088/1674-1056/27/8/087303

1. Introduction

Two-dimensional (2D) materials, such as graphene, transition-metal dichalcogenides (TMDs), and hexagonal boron nitride (h-BN), have rapidly developed as intriguing building blocks for various optoelectronic and electronic devices, including quantum sources,[1,2] optical modulators,[3] polarizers,[4] field-effect transistors,[5] and photodetectors[6–9] owing to their unique optical and electronic properties.[10–15] Compared with the zero-bandgap graphene, monolayer TMDs have direct bandgaps, such as 1L-MoS_2 (1.9 eV) and 1L-WSe_2 (∼1.65 eV), which have high light absorbance in the visible range.[16–18] However, it is also their semiconducting nature that leads to the difficulty in making good ohmic contacts on these materials, as high contact resistance caused by schottky barriers is often formed at the metal-TMD interfaces.[19,20] Reducing the Schottky barrier at metal-TMD interfaces then becomes a critical issue toward further improving the transport performance of TMD-based devices. A promising solution to this problem is to incorporate graphene into TMDs to form hybrid heterojunctions, in which graphene layers are used as work-function tunable electrodes while TMDs behave as photoactive materials that provide strong light-matter interaction and photon absorption. Experimental progress in such photodetectors has been made for both in-plane and out-of-plane layouts.[21–23] Although the bias field in out-of-plane devices can be much higher (up to ∼ 1 V·nm^{-1}),[24] the in-plane devices allow for better control of material properties through electrostatic gating.

In this paper, we present an in-plane monolayer WSe_2 p–n junction device fabricated based on a polycarbonates dry transfer method.[25,26] We utilize graphite as electrodes to avoid the monolayer WSe_2 directly being exposed to electron-beam, which has been reported to be able to degrade the overall quality of this sensitive crystal.[27,28] Recently, in a similar study hydrazine was used to locally dope WSe_2 to define a p–n junction.[29] Here we demonstrate a low-power dissipation in-plane WSe_2 p–n junction device through showing an ambipolar behavior with a reduced threshold voltage by a factor of two compared with the previous results on lateral electrostatically doped WSe_2 p–n junction.[9,23,30] Upon optical illumination, this device demonstrates a photoresponsivity of 0.12 mA·W^{-1} and a maximum external quantum efficiency of 0.03%. Our

*Project supported by the National Key Research and Development Program of China (Grant No. 2016YFA0301700), the National Natural Science Foundation of China (Grant Nos. 61590932, 11774333, 61674132, 11674300, 11575172, and 11625419), the Anhui Provincial Initiative in Quantum Information Technologies, China (Grant Nos. AHY080000 and AHY130300), the Strategic Priority Research Program of the Chinese Academy of Sciences (Grant No. XDB24030601), and the Fundamental Research Funds for the Central Universities, China. This work was partially carried out at the USTC Center for Micro and Nanoscale Research and Fabrication.

†Corresponding author. E-mail: renxf@ustc.edu.cn
‡Corresponding author. E-mail: gpguo@ustc.edu.cn

© 2018 Chinese Physical Society and IOP Publishing Ltd

studies set an example for designing the next-generation flexible, transparent, and low-power dissipation two-dimensional optoelectronic devices.

2. Fabrication

Figure 1(a) illustrates the fabrication procedure for our monolayer WSe_2 p–n junction device. A thin film of polycarbonate (PC, Sigma Aldrich, 6% in weight dissolved in chloroform) was used to cover a piece (1 nm×1 mm) of polydimethylsiloxane (PDMS), which was initially placed on a glass slide. After that, the slide was positioned upside down to pick up a pre-prepared top-layer h-BN, as shown in Fig. 1(a(i)), using the expansion/contraction of the PC film controlled by the precise temperature-step from 40 °C to 120 °C. The top-layer h-BN was then used to pick up the graphite which was previously etched into three stripes from an original piece (Fig. 1(a(ii)). These stripes were used as source/drain electrodes in our device, avoiding the WSe_2 directly exposed to the e-beam. Subsequently, a monolayer WSe_2 and another layer of h-BN were picked up (Fig. 1(a(iii)), eventually forming an h-BN-graphite-WSe_2-h-BN stack, as shown in Fig. 1(a(iv)). Finally, we transferred the stack onto the Si/SiO_2 substrate with pre-patternedTi/Au gate electrodes, and then washed out the PC in chloroform, as shown in Fig. 1(b). Here, the graphite and h-BN flakes were mechanically exfoliated (using scotch tape) and placed on the substrate (SiO_2/Si). Both graphite and h-BN flakes were annealed at 400 °C for 2 h (under H_2/Ar atmosphere with 1:30 ratio) to eliminate the tape residue. Monolayer WSe_2 was exfoliated using PDMS as a tape to increase the yielding. The single crystalline graphite and WSe_2 are bought from SPI Supplies and HQ Graphene, respectively.

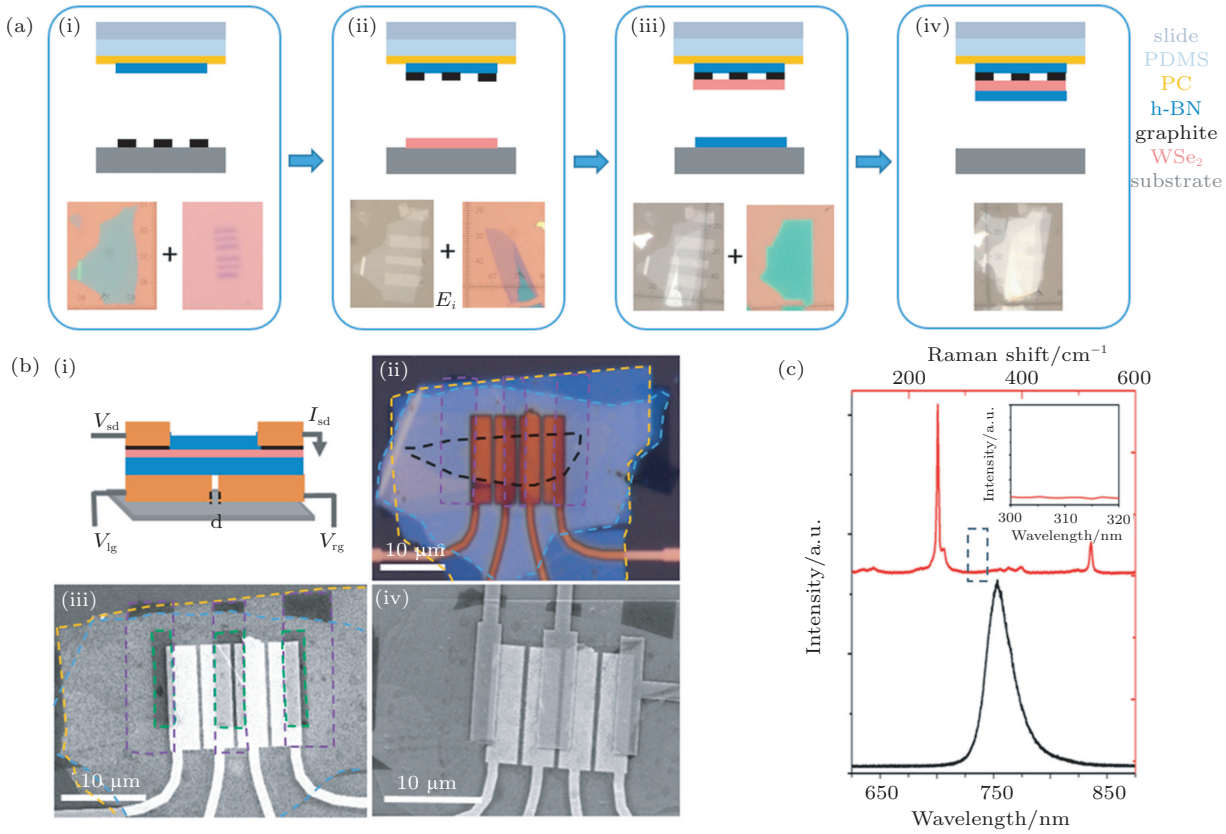


Fig. 1. (color online) (a) Van der Waals pick-up transfer process. (b) (i) Lateral view and (ii) optical microscope image of the monolayer WSe_2 p–n junction device. (d = 500 nm, black dashed line: outline of monolayer WSe_2, yellow dashed line: outline of bottom-layer h-BN, cyan dashed line: outline of top-layer h-BN, purple dashed line: outline of graphite, gold area: separated bottom gates.) (iii) SEM image after etching top-layer h-BN (green dashed line: outline of graphite after etching top-layer h-BN). (iv) SEM image after evaporation *in-situ*. (c) Raman shift and PL spectrum, showing the characteristic of monolayer WSe_2, with inset indicating the magnified gray dotted line area. The unit a.u. is short for arb. units.

Figures 1(b(i)–1(b(ii)) show the lateral view and the optical microscope image of the device studied in this letter. The gap of two separated electrostatic-gates is about 500 nm.[23] To eliminate the residues of undissolved PC film and hence to reduce the contact resistance, we etched away the top h-BN layer (which covers the three graphite electrodes) (Fig. 1(b(iii))) by O_2 (4 sccm) mixed with CHF_3 (40 sccm) under an RF power of 200 W, and deposited Ti/Au (5 nm/45 nm) in situ (Fig. 1(b(iv))) by standard e-beam evaporation. As a result, the majority of monolayer WSe_2 was not exposed to the high energy e-beam. Figure 1(c) shows the Raman shift and photoluminescence (PL) spectrum of monolayer WSe_2. The Raman spectrum measurement was performed with a Jobin–Yvon Horiba HR800 micro-Raman spectrometer with 514-nm excitation laser at room temperature. A 100×objective lens (NA = 0.9) with an accumulation time of 10 s was used for Ra-

man data collection. PL measurement was performed with a Princeton Instrument Acton SP2500 spectrograph with 532-nm excitation laser at room temperature. A 100×objective lens (NA = 0.9) with an accumulation time of 2 s was used for PL data collection. To prevent the samples from overheating, the power of excitation laser was kept under 1 mW for all experiments. The typical Raman spectrum for monolayer WSe_2, in the absence of the peak around 308 cm^{-1} (inset of Fig. 1(c)), was clearly seen.[31] The peak around 750 nm in the PL spectrum was also consistent with a previous result.[32]

3. Results and discussion

A schematic diagram of the measurement setup is presented in the inset of Fig. 2(a), with a bias voltage V_b applied to the source electrode and the DC current I_{sd} through the device measured at the drain electrode. All measurements are performed at room temperature and atmosphere pressure. The local carrier density in our monolayer WSe_2 p–n junction device can be independently tuned by the voltages applied to the two bottom gates i.e., V_{lg} for the left gate and V_{rg} for the right gate. In this manner, different doping configurations can be achieved in our device. As shown in Fig. 2(a), the current in linear scale (black curve) and the current in logarithmic scale (blue curve) both exhibit an ambipolar dependence on the gate voltage ($V_{lg} = V_{rg} = V_g$) at a bias voltage of $V_{sd} = 500$ mV. Here the relatively low on-off ratio observed is due to the choice of sensitivity set-up in SR570 preamplifer. The characteristics of conductance are similar to previous results controlled by an overall electrostatic gating.[33] It indicates that this device can be tuned from an electron-doped regime to a hole-doped regime by two separated electrostatic-gates. We then adjust V_{lg} and V_{rg} to reach different doping regimes and measure the current as a function of bias voltage as displayed in Fig. 2(b). The black curve shows that our device is of p-type when both V_{lg} and V_{rg} are negative. The device can operate as a diode to rectify the current when the voltages applied to the two bottom gates are opposite to each other. The NP junction shows higher contact resistance than the PN junction, which is probably due to the different Schottky barrier heights arising from the asymmetrical p–n threshold voltage on each side of the bottom gate.

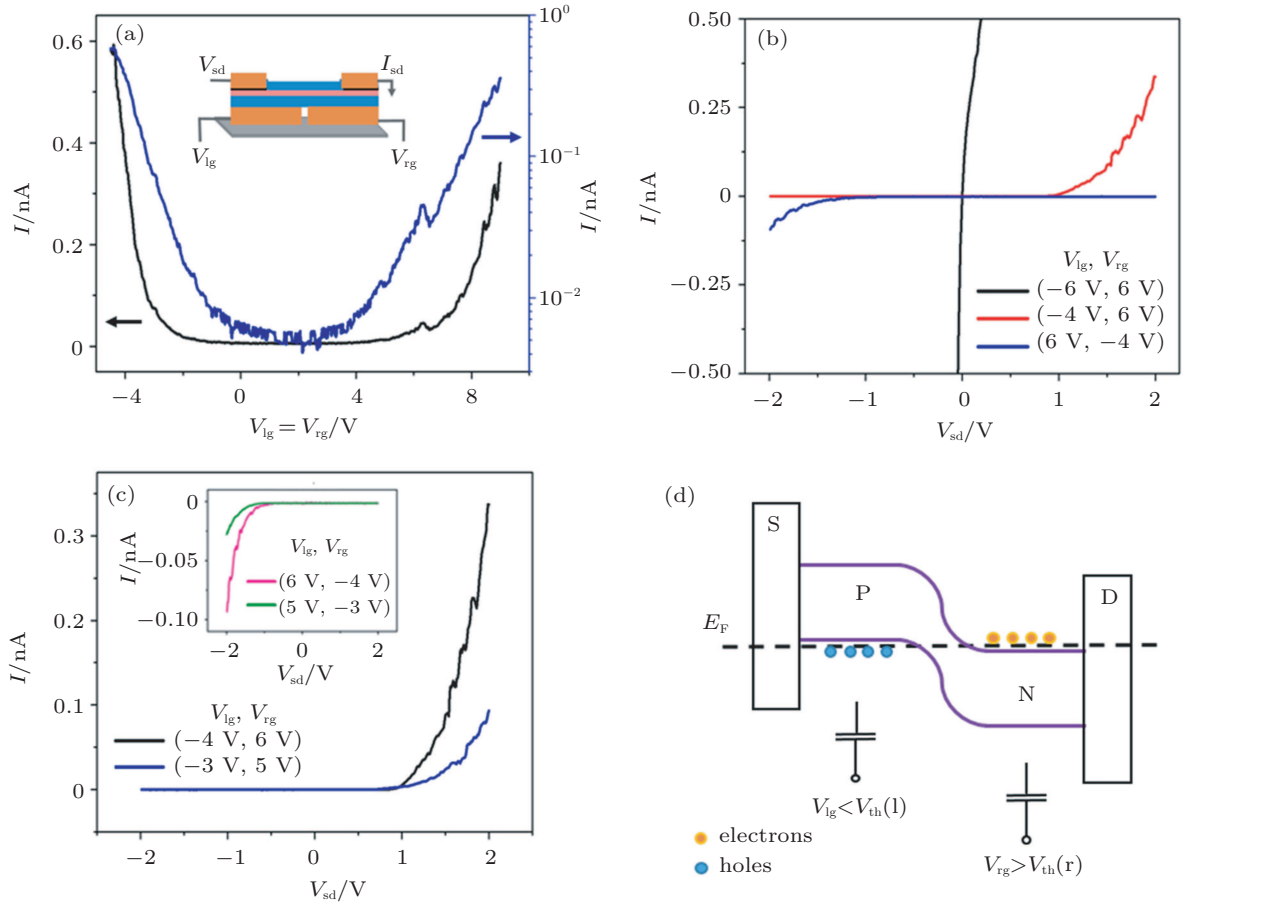


Fig. 2. (color online) (a) Variation of the current in linear scale (black curve) and the current in logarithmic scale (blue curve) with both bottom gate voltages ($V_{lg} = V_{rg} = V_g$) at voltage bias $V_{sd} = 500$ mV, showing an ambipolar behavior expected for a semiconductor. (b) *I*–*V* characteristics of the monolayer WSe_2 p–n junction device in the dark for different doping configurations: black curve: $V_{lg} = V_{rg} = -6$ V (PP), red curve: $V_{lg} = -4$ V, $V_{rg} = 6$ V (PN), blue curve: $V_{lg} = 6$ V, $V_{rg} = -4$ V (NP). (c) Main panel: *I*–*V* characteristics at different PN junction fields as controlled by the two bottom split-gate voltages (black curve: $V_{lg} = -4$ V, $V_{rg} = 6$ V; blue curve: $V_{lg} = -3$ V, $V_{rg} = 5$ V). Inset panel: *I*–*V* characteristics at different NP junction fields (magenta curve: $V_{lg} = 6$ V, $V_{rg} = -4$ V; green curve: $V_{lg} = 5$ V, $V_{rg} = -3$ V). (d) Schematic band diagram of the WSe_2 junction in the PN regime showing a distortion of the WSe_2's band V_{th}(l) and V_{th}(r), denoting two threshold voltages of bottom gates which can tune the WSe_2 to p-type and n-type regimes respectively, are estimated from the current in logarithmic scale (blue curve) shown in Fig. 2(a).

Figure 2(c) shows the stable carrier currents of our device as a diode under different junction configurations. In the main panel, the current–voltage characteristics are shown at different PN junction fields. The inset panel shows the current–voltage characteristics in different NP junction fields. There are two threshold voltages of bottom gates, i.e., $V_{\rm th}$(l) and $V_{\rm th}$(r), for p-type and n-type regimes respectively in Fig. 2(a). From the current in logarithmic scale (blue curve), we can estimate the $V_{\rm th}$(l) at about -1 V and the $V_{\rm th}$(r) at about 4 V. As an example, the schematic band diagram of the PN junction is illustrated in Fig. 2(d). When $V_{\rm lg}$ is less than $V_{\rm th}$(l), the left-side WSe_2 is tuned to a p-type region. On the other hand, when $V_{\rm rg}$ is larger than $V_{\rm th}$(r), the right-side WSe_2 is tuned to an n-type region. Therefore, by applying different gate voltages to the left and right bottom gates, we can tune the junction field and study the optoelectronic properties of our device.

We perform the optoelectronic experiments on a monolayer WSe_2 p–n junction device by using the scanning photocurrent microsystem as shown in Fig. 3(a). We excite the WSe_2 with 532-nm laser (beam diameter $\sim$700 nm, power 2 μW), and collect the photoluminescence (PL) of WSe_2 through a 550-nm long pass filter. We perform the photocurrent measurements by focusing the laser spot at the middle of WSe_2 (in between the two bottom gates). Figure 3(b) shows the current–voltage relations of the device in the PN regime ($V_{\rm lg} = -4$ V, $V_{\rm rg} = 6$ V) in the dark (black empty square) and under illumination with a wavelength of 532 nm, power of 2 μW, and spot diameter of $\sim$700 nm (red empty circle). It clearly shows that a reverse current is generated upon laser illumination at negative bias. The origin is explained in Fig. 3(c) as follows. When the laser is injected, direct-bandgap WSe_2 causes the intrinsic absorption of photons whose energy is larger than the bandgap of WSe_2, generating electron–hole pairs distributed in the PN junction. As the electron–hole pairs accumulate, more electrons from the P region move to the N region and more holes from the N region move to the P region. Such a carrier density change leads to the increase of photocurrent in the PN junction. The photodetector operation is in the third quadrant in Fig. 3(b), in which the current and voltage have the same sign (negative) and hence the device dissipates power. However, if a positive voltage is applied to the diode while light is incident on the junction, the sign of the current is negative, indicating that the diode is a source of power rather than a dissipater of power. This is the regime of operation of the solar cell as shown in the fourth quadrant of the I–V plane in Fig. 3(b).

We further measure the photocurrent of PN junction ($V_{\rm lg} = -4$ V, $V_{\rm rg} = 6$ V) under the illumination of 532-nm laser at different power levels (Fig. 4(a)). We treat the photocurrent as the dark current when excitation power is zero.

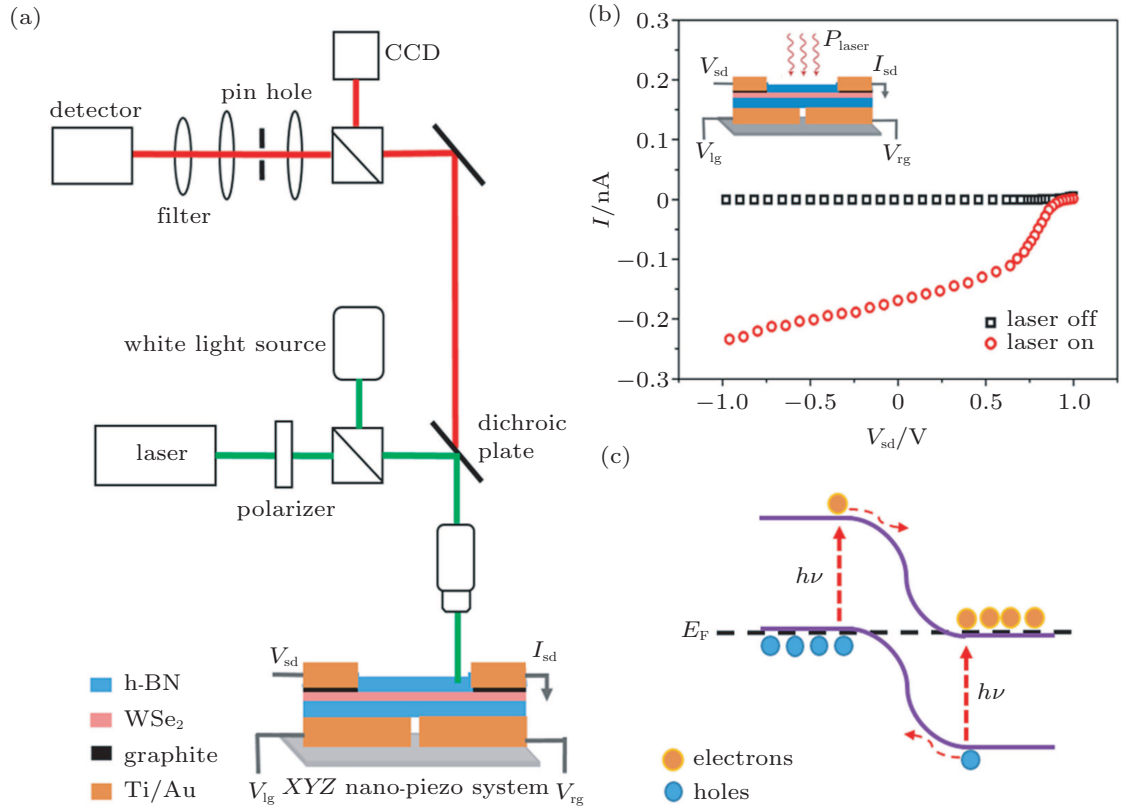


Fig. 3. (color online) (a) Experimental setup used to measure photocurrent and PL in our WSe_2 PN junction. (b) The I–V curve of the device in the PN regime ($V_{\rm lg} = -4$ V, $V_{\rm rg} = 6$ V) in the dark and the I–V curve under a laser exposure (2 μW) in the middle of the WSe_2. (c) Schematic band diagrams of the WSe_2 PN junction under laser exciting.

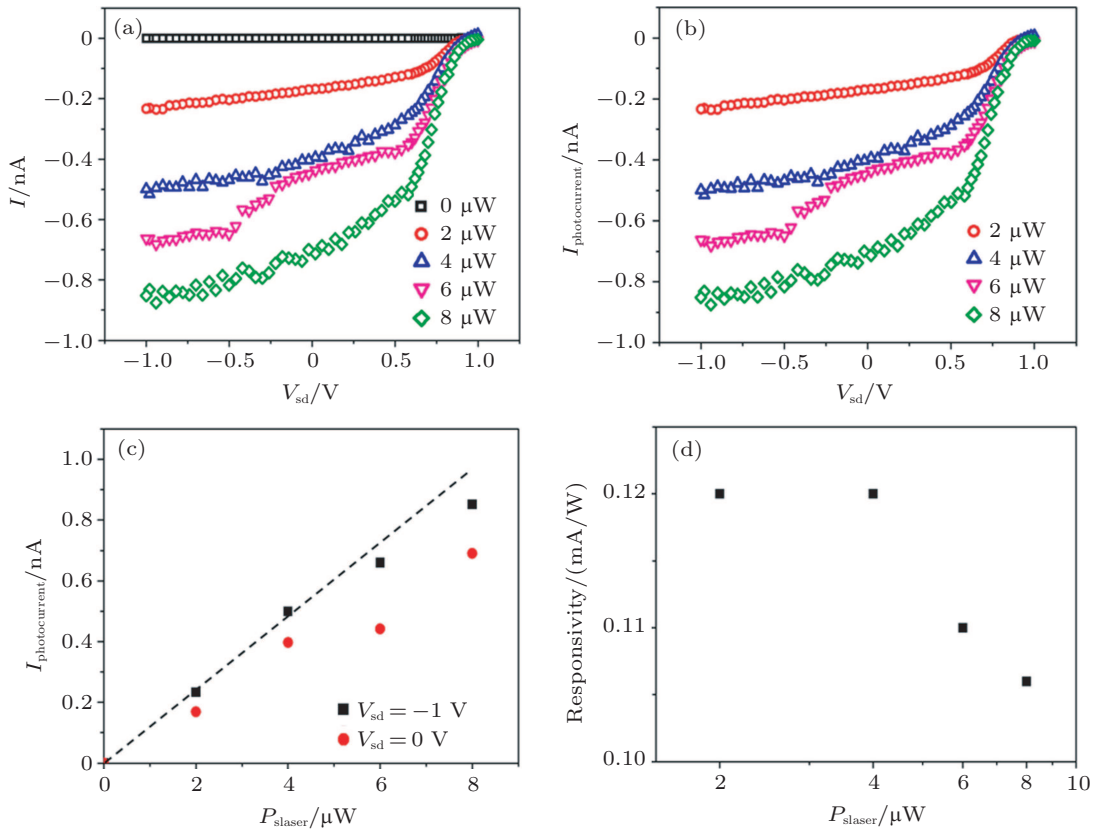


Fig. 4. (color online) Optoelectronic characterization of the PN junction ($V_{lg} = -4$ V, $V_{rg} = 6$ V) excited by a 532-nm diode laser, showing (a) current–voltage of source–drain relation under different laser powers, (b) photocurrents of PN junction under different laser powers, (c) photocurrent as a function of laser power under different bias voltages, and (d) photoresponsivity versus laser power in the PN junction region.

In order to analyze the data, we deduct the dark current from the measured photocurrent, which is shown in Fig. 4(b). Under negative bias,the photocurrent has strong dependence on incident power. We show the plots of the extracted photocurrent I_{ph} versus excitation power at two different V_{sd} values in Fig. 4(c), where a linear fit of I_{ph} for $V_{sd} = 1$ V is also presented. The sublinear response to the excitation power indicates the recombination of the photogenerated carriers, which may be related to the intrinsic defects and impurities of the WSe_2.[34,35] When $V_{sd} = 0$ V, the p–n diode is a short circuit, indicating that the photocurrent in this regime results mainly from the incident photons.[23,36] From Fig. 4(c), we obtain the photoresponsivity of our device, which is defined as the ratio between the photocurrent and the excitation power. As plotted in Fig. 4(d), the maximum photoresponsivity is 0.12 mA/W, and corresponds to an external quantum efficiency (EQE = photoresponsivity $*hc/\lambda e$) of 0.03%. Here the photoresponsivity and EQE are low compared with previous results about the lateral electrostatically doped WSe_2 p–n homojunction.[9,23,30,37] The reason may be as follows. Firstly, the bubbles formed in the PC transfer process could affect the effective carrier transfer between different layers. Secondly, the etching process for the top-layer h-BN may produce some residues on the graphite and hence introduce extra barriers between graphite and the subsequently deposited electrodes. Nevertheless, for the WSe_2 located in the middle layer, the intrinsic defects should be improved due to the sandwiched structure.[26] Although the quality and interface of WSe_2 are decent enough and the contact resistance between WSe_2 and other material is low, the EQE in lateral electrostatically doped WSe_2 p–n junction may be lower than those observed in many vertical heterostructure devices. This is because the electrostatic doping exhibits a spatial gradient, which has an effect on the diffusion of electrons and holes. In contrast, the atomically sharp junctions in the vertical heterostructure devices can enhance efficiency for charge separation.[37] We expect that vertical junctions could increase the photoresponsivity and EQE by more than an order of magnitude.[9]

4. Conclusions

In this work, we have demonstrated an in-plane monolayer WSe_2 p–n junction device which is tunable by two separated electrostatic-gates. The device is fabricated by the PC dry transfer method to protect the monolayer WSe_2 from direct exposure to electron-beam in order to maintain the quality of crystal. Upon optical illumination, this device gives a maximum photoresponsivity of 0.12 mA/W and an external

quantum efficiency of 0.03%. Although suspected extrinsic effects such as impurity and defect states restrict the performance of our in-plane photodetector, our study shows that its operation is robust and fully tunable. The device can be tuned by two pre-patterned electrostatic-gates and shows an ambipolar behavior with the threshold voltage decreasing by a factor of two, compared with previous results about the lateral electrostatically doped WSe_2 p–n homojunction.[9,23,30] In conclusion, we demonstrate a low-power dissipation p–n photodetector, which is promising for designing the next-generation optoelectronic devices. In the future, studies that clarify the intrinsic and extrinsic mechanisms are required in order to optimize the structures for better performances.

Acknowledgement

This work was partially carried out at the USTC center for Micoscale Research and Fabrication.

References

[1] He Y M, Clark G, Schaibley J R, He Y, Chen M C, Wei Y J, Ding X, Zhang Q, Yao W, Xu X, Lu C Y and Pan J W 2015 *Nat. Nanotechnol.* **10** 497
[2] Tran T T, Bray K, Ford M J, Toth M and Aharonovich I 2016 *Nat. Nanotechnol.* **11** 37
[3] Liu M, Yin X, Ulin-Avila E, Geng B, Zentgraf T, Ju L, Wang F and Zhang X 2011 *Nature* **474** 64
[4] Bao Q, Zhang H, Wang B, Ni Z, Lim C H Y X, Wang Y, Tang D Y and Loh K P 2011 *Nat. Photon.* **5** 411
[5] Radisavljevic B, Radenovic A, Brivio J, Giacometti I V and Kis A 2011 *Nat. Nanotechnol.* **6** 147
[6] Koppens F H L, Mueller T, Avouris P, Ferrari A C, Vitiello M S and Polini M 2014 *Nat. Nanotechnol.* **9** 780
[7] Xia F, Mueller T, Lin Y M, Valdes-Garcia A and Avouris P 2009 *Nat. Nanotechnol.* **4** 839
[8] Britnell L, Ribeiro R, Eckmann A, Jalil R, Belle B, Mishchenko A, Kim Y J, Gorbachev R, Georgiou T and Morozov S 2013 *Science* **340** 1311
[9] Baugher B W, Churchill H O, Yang Y and Jarillo-Herrero P 2014 *Nat. Nanotechnol.* **9** 262
[10] Geim A K and Novoselov K S 2007 *Nat. Mater.* **6** 183
[11] Wang Q H, Kalantar-Zadeh K, Kis A, Coleman J N and Strano M S 2012 *Nat. Nanotechnol.* **7** 699
[12] Fiori G, Bonaccorso F, Iannaccone G, Palacios T, Neumaier D, Seabaugh A, BanerjeeS K and Colombo L 2014 *Nat. Nanotechnol.* **9** 768
[13] Song X X, Liu D, Mosallanejad V, You J, Han T Y, Chen D T, Li H O, Cao G, Xiao M, Guo G C and Guo G P 2015 *Nanoscale* **7** 16867
[14] Song X X, Zhang Z Z, You J, Liu D, Li H O, Cao G, Xiao M and Guo G P 2015 *Sci. Rep.* **5** 16113
[15] Liu D, Yu L, Xiong X, Yang L, Li Y, Li M, Li H O, Cao G, Xiao M, Xiang B, Min C J, Guo G C, Ren X F and Guo G P 2016 *Opt. Express* **24** 27554
[16] Bernardi M, Palummo M and Grossman J C 2013 *Nano Lett.* **13** 3664
[17] Li Y, Chernikov A, Zhang X, Rigosi A, Hill H M, van der Zande A M, Chenet D A, Shih E M, Hone J and Heinz T F 2014 *Phys. Rev. B* **90** 205422
[18] Funke S, Miller B, Parzinger E, Thiesen P, Holleitner A W and Wurstbauer U 2016 *J. Phys.: Condens. Matter* **28** 385301
[19] Chuang H J, Tan X, Ghimire N J, Perera M M, Chamlagain B, Cheng M C, Yan J, Mandrus D, Tománek D and Zhou Z 2014 *Nano Lett.* **14** 3594
[20] Fang H, Chuang S, Chang T C, Takei K, Takahashi T and Javey A 2012 *Nano Lett.* **12** 3788
[21] Lopez-Sanchez O, Lembke D, Kayci M, Radenovic A and Kis A 2013 *Nat. Nanotechnol.* **8** 497
[22] Lee C H, Lee G H, Van Der Zande A M, Chen W, Li Y, Han M, Cui X, Arefe G, Nuckolls C, Heinz T F, Guo J, Hone J and Kim P 2014 *Nat. Nanotechnol.* **9** 676
[23] Pospischil A, Furchi M M and Mueller T 2014 *Nat. Nanotech.* **9** 257
[24] Mak K F and Shan J 2016 *Nat. Photon.* **10** 216
[25] Dean C R, Young A F, Meric I, Lee C, Wang L, Sorgenfrei S, Watanabe K, Taniguchi T, Kim P, Shepard K L and Hone J 2010 *Nat. Nanotechnol.* **5** 722
[26] Wang L, Meric I, Huang P Y, Gao Q, Gao Y, Tran H, Taniguchi T, Watanabe K, Campos L M, Muller D A, Guo J, Kim P, Hone J, Shepard K L and DeanC R 2013 *Science* **342** 614
[27] Kang J, Lee S and Choi B 2016 *Jpn. J. Appl. Phys.* **55** 111301
[28] Puster M, Rodríguez-Manzo J A, Balan A and Drndic M 2013 *ACS Nano* **7** 11283
[29] Sun M, Xie D, Sun Y, LiWand Ren T 2017 *Nanotechnology* **29** 015203
[30] Ross J S, Klement P, Jones A M, Ghimire N J, Yan J, Mandrus D G, Taniguchi T, Watanabe K, KitamuraK, Yao W, Cobden D H and Xu X 2014 *Nat. Nanotechnol.* **9** 268
[31] ZhaoW, Ghorannevis Z, Amara K K, Pang J R, Toh M, Zhang X, Kloc C, Tan P H and Eda G 2013 *Nanoscale* **5** 9677
[32] He K, Kumar N, Zhao L, Wang Z, Mak K F, Zhao H and Shan J 2014 *Phys. Rev. Lett.* **113** 026803
[33] Allain A and Kis A 2014 *ACS Nano* **8** 7180
[34] Zhou X, Zhou N, Li C, Song H, Zhang Q, Hu X, Gan L, Li H, Lu J and Luo J 2017 *2D Mater.* **4** 025048
[35] Zhang W, Huang J K, Chen C H, Chang Y H, Cheng Y J and Li L J 2013 *Adv. Mater.* **25** 3456
[36] Furchi M M, Pospischil A, Libisch F, Burgdörfer J and Mueller T 2014 *Nano Lett.* **14** 4785
[37] Cheng R, Li D, Zhou H, Wang C, Yin A, Jiang S, Liu Y, Chen Y, Huang Y and Duan X 2014 *Nano Lett.* **14** 5590